THE JOURNAL OF PHYSICAL CHEMISTRY LETTERS
A JOURNAL OF THE AMERICAN CHEMICAL SOCIETY

pubs.acs.org/JPCL

Letter

Polyacetylene Revisited: A Computational Study of the Molecular Engineering of N-type Polyacetylene

Liam D. P. Foyle, Garion E. J. Hicks, Adam A. Pollit, and Dwight S. Seferos*

Cite This: *J. Phys. Chem. Lett.* 2021, 12, 7745–7751

Read Online

ACCESS | Metrics & More | Article Recommendations | Supporting Information

ABSTRACT: The development of stable and highly conductive polymers, particularly *n*-type materials, remains an outstanding challenge in organic electronics. *N*-doped polyacetylene has long been studied as a highly conductive organic *n*-type material but suffers from extremely poor stability. Herein, we use DFT to model a series of *n*-doped polyacetylene derivatives, which have been functionalized with a range of electron-withdrawing substituents, with the goal of identifying attractive candidates for synthesis. We analyze the predicted molecular orbital energies, polymer planarity, and delocalization of charge carriers along the polymer backbone. In so doing, we develop key insights about the ideal substituents for both stable and highly conductive polyacetylene derivatives. This work will inform the modern synthesis and development of new polyacetylene derivatives. Beyond this, the work identifies a variety of new materials that have not yet been synthesized and should be good candidates for emerging optoelectronic applications including soft thermoelectrics, bioelectronics, and flexible device technologies.

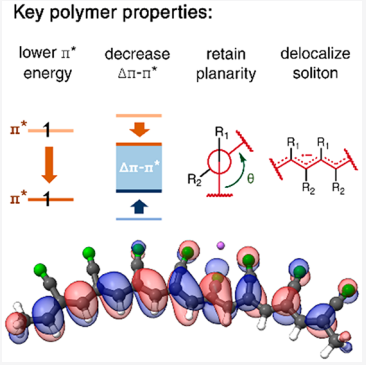

Organic electronics have been studied for the past 60 years for their promise as lightweight, flexible, nontoxic materials[1] and their potential as biodegradable or recyclable materials within a circular economy.[2−4] Interest in recent decades has focused on semiconductors, which have many applications including photovoltaics, light emitting diodes, and field effect transistors.[5] On the other hand, the development of highly conductive organic materials, or "Synthetic Metals," has remained an outstanding challenge.[6] Such materials would be of interest for a range of applications that are complementary to their semiconducting counterparts, including printable and stretchable conductors,[7,8] transparent electrodes,[9,10] thermoelectric generators,[11] and biocompatible electronics.[12−14]

Redox doping is a promising strategy for accessing high-conductivity organic materials.[15,16] Whereas inorganic semiconductors are typically doped with small quantities of electron-rich or electron-poor elements, organic materials are doped with molecular oxidants or reductants to afford *p*- or *n*-type materials, respectively. *p*-Type doping (*p*-doping) involves removing electrons from the occupied bonding orbitals to create delocalized holes, while *n*-doping involves adding electrons to low-lying antibonding unoccupied states to form mobile charge carriers.[17] Redox doping typically requires that >33% of the polymer chain active sites are charged to achieve high conductivity and operates by both increasing the number of delocalized charge carriers and decreasing energy barriers between charge wells to create efficient charge-transport pathways. This can result in an increase in conductivity, for example, from 10^{-5} to 10^{5} S/cm with *p*-doping, and from 10^{-5} to 10^{3} S/cm with *n*-doping.[18] However, doped organic materials are often less stable than their undoped precursors, with *n*-type materials often suffering from extremely short lifetimes.[5] This has caused *n*-type materials to lag behind their *p*-type counterparts in their development and application.

Polyacetylene was the first organic polymer to exhibit metal-like conductivities.[19] MacDiarmid, Heeger, Shirakawa, and co-workers discovered in the 1970s that polyacetylene changed from a semiconductor to conductor upon addition of either an oxidant (I_2) or a reductant (sodium naphthalenide) to *p*- or *n*-dope the polymer, respectively.[20,21] They also found that *p*-doping with I_2 could vary the conductivity of polyacetylene by 11 orders of magnitude.[21] Unfortunately, redox doped polyacetylene is very unstable, resulting in short device lifetimes which limited further study. Additionally, there have been challenges to synthesizing polyacetylene in a controlled manner, which would facilitate structural modifications that could improve material properties. However, recent work has demonstrated the synthesis of polyacetylene derivatives by a variety of methods,[22−26] including soluble, ionically functionalized derivatives used to fabricate p/n junctions,[27,28] making it an ideal candidate for further exploration.

Herein, we use DFT to model the effect of functionalizing polyacetylenes with electron withdrawing groups that stabilize *n*-type doping (Figure 1). DFT has become an increasingly

Received: June 16, 2021
Accepted: August 2, 2021
Published: August 9, 2021

https://doi.org/10.1021/acs.jpclett.1c01925
J. Phys. Chem. Lett. 2021, 12, 7745–7751

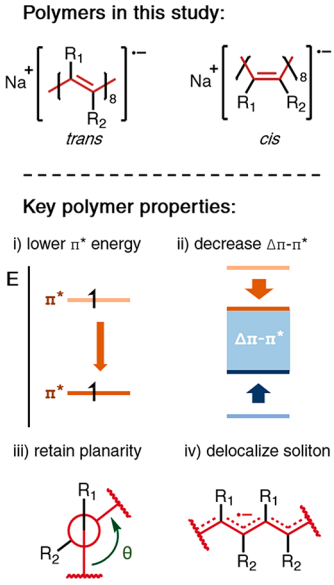

Figure 1. Modeling *n*-doped polyacetylenes. Polymers are modeled in either their *cis* or *trans* isomers, determined by which isomer possesses the lowest total energy. R_1/R_2 = H, ME, PFP, *p*NP, CF_3, CF_2CF_3, CN. Polymer properties that are associated with stability and high conductivity (bottom) are analyzed to identify top candidates for synthesis.

utilized tool for understanding complex and unstable doped polymers.[29,30] The goal of this study is to identify promising *n*-dopable polyacetylene derivatives as synthetic targets, focusing on key features that can promote the stabilization of *n*-doped polyacetylenes and high conductivity in device applications. To do this, we examine singly reduced mono- and disubstituted polyacetylenes functionalized with electron withdrawing groups and sodium counterions to simulate the doping of polyacetylene with sodium naphthalenide.[5]

Our aim is to identify polymers that are stable and are highly conductive upon doping. To this end, we selected four criteria: (i) lowering the π^* orbital energy, (ii) retaining polymer planarity, (iii) decreasing the $\pi-\pi^*$ molecular orbital energy difference ($\Delta\pi-\pi^*$), and (iv) increasing soliton delocalization (Figure 1). Decreasing the π^* energy (i) is meant to prevent oxidation and degradation under ambient conditions.[31] In previous studies, n-doped polyacetylene has proven difficult to work with because it reacts readily with oxygen and water.[32] High planarity (ii) and a narrow $\Delta\pi-\pi^*$ (iii) are thought to be associated with increased polymer charge mobility.[33] Lastly, we consider the effect of delocalized charge carrier (soliton) formation (iv) because broad, delocalized solitons are important for rapid charge transport in doped polyacetylenes.[34] We studied a range of electron withdrawing groups as substituents, including methyl ester (ME), pentafluorophenyl (PFP), *p*-nitrophenyl (*p*NP), trifluoromethyl (CF_3), pentafluoroethyl (CF_2CF_3), and cyano (CN). As polyacetylene exists as both *cis* and *trans* isomers, the most stable polymer conformation was taken to be the most likely to form and thus included here. See the Supporting Information (SI) for data on both *cis* and *trans* isomers (Table S1).

We first validated this method by comparing calculated π and π^* orbital energies with experimentally determined redox properties. By this method, polyacetylene is modeled with eight repeat units in the presence of a sodium atom; the system is then optimized in a doublet state such that charge is transferred to the polyacetylene backbone and the sodium cation migrates to stabilize the resulting soliton. We find a singly occupied π^* orbital energy of −3.3 eV (Figure 2). *trans*-

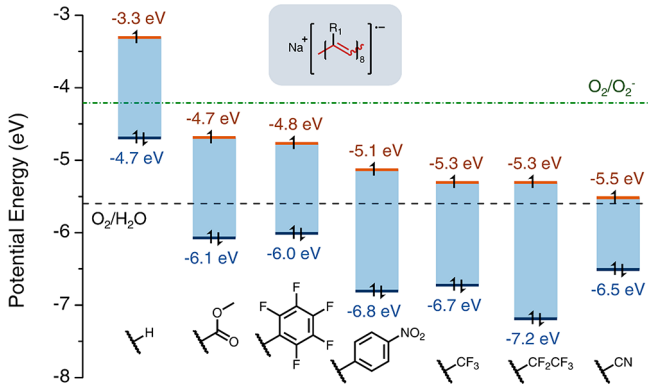

Figure 2. Potential energy diagram of monosubstituted polyacetylene derivatives. Calculated MO energies of the π (blue) and π^* (orange) orbitals for each polyacetylene derivative. Calculations performed on the polyacetylene derivative doped with Na in the doublet state. The dotted lines indicate the energy relative to the absolute potential energy of SHE for the reduction of O_2 gas in water under neutral (green) or acidic (black) conditions.

Polyacetylene has a reduction potential of 1.46 V vs Na/Na^+,[35] which corresponds to an absolute reduction potential[36] (i.e., relative to vacuum) of −3.38 eV, in close agreement with the calculated value. The experimental electrochemical bandgap for *trans*-polyacetylene of 1.51 eV[35] compares well with the calculated $\Delta\pi-\pi^*$ of 1.4 eV. This slight underestimation of the bandgap could potentially result from either disorder in polymer films or interactions with solvent decreasing polymer planarity and increasing $\Delta\pi-\pi^*$. Overall, this suggests that the computational method is sufficiently robust to effectively model polyacetylene and its derivatives.

To evaluate the stability of the *n*-doped polyacetylene derivatives, we compared their π^* orbital energies against the reduction potential of O_2. The most important decay pathway for *n*-doped polymers is oxidation by O_2, as it precludes their study under anything but the most stringent, air-free conditions.[31] However, the reduction potential of O_2 depends strongly on the environment.[37] In polar aprotic solutions such as acetonitrile, O_2 is reduced to the superoxide anion at an absolute potential of −3.99 eV,[38] whereas in water (pH = 7) this occurs at −4.21 eV (Figure 2, green dotted line). We expect that oxidation of the polymer upon exposure to atmospheric conditions would occur rapidly if the singly occupied π^* orbital has a higher absolute potential than this. Under acidic conditions, O_2 is reduced to form H_2O; this is significantly more favorable, and reduction occurs above −5.6 eV (Figure 2, black dotted line). Of course, it is unlikely that the unprotected, *n*-doped polymer would be submerged in an acidic solution. We therefore expect that π^* orbitals near or below −5.6 eV would be unlikely to react under most experimental conditions. It should be noted that photoinduced oxidative degradation by O_2 is also common in π-conjugated polymers.[39−41] Although this is difficult to model looking at orbital potential energies alone, a lower energy π^* orbital is nevertheless more stable and less likely to exhibit unwanted reactivity.

All monosubstituted polyacetylene derivatives in this study possess calculated π^* orbital energies below O_2 reduction

https://doi.org/10.1021/acs.jpclett.1c01925
J. Phys. Chem. Lett. 2021, 12, 7745−7751

under neutral conditions (Figure 2). CN-substituted polyacetylene has the lowest energy π^* orbital at −5.5 eV, nearly the same potential energy as O_2 reduction under acidic conditions. There are three key features that explain this finding: electronegativity, resonance, and size. Intuitively, stronger electron withdrawing substituents should provide the strongest inductive stabilization. We hypothesize that *p*NP-substituted polyacetylene exhibits a 0.3 eV greater π^* orbital stabilization than PFP-substituted polyacetylene due to the combined effects of greater electronegativity and resonance stabilization from the nitro-group. The ME functionality, being moderately bulky while also providing less resonance and inductive stabilization, appears to afford the least stabilized π^* orbital. The smaller (but still fluorinated) CF_3 group provides even greater stabilization than either phenyl or ester functionalities, resulting in a lower polyacetylene π^* orbital energy. This implies that substituent size plays an important role in determining orbital energies. To examine this further, we decided to study the effect of substituent size on $\Delta\pi-\pi^*$ and polymer planarity.

$\Delta\pi-\pi^*$ and polymer planarity are important factors that affect charge-transport. Planarity has been shown to affect both intermolecular and intramolecular interactions in other π-conjugated polymers. Structural rigidification to increase planarity is associated with a decrease in $\Delta\pi-\pi^*$ due to improved alignment between adjacent π-bonds.[42,43] Insofar as planarity and a narrow $\Delta\pi-\pi^*$ are associated with π-orbital alignment into larger, delocalized π-systems, these factors are also associated with improved charge transport.[44] Increased planarity is also associated with improved solid-state polymer order, which has been shown to improve conductivity in redox doped π-conjugated polymers.[45] More precisely, the presence of crystalline tie-chains between polymers in a semicrystalline or largely amorphous matrix are believed to facilitate intermolecular charge hopping.[46] While polymer crystallization depends on a range of factors, including processing conditions and side chain geometry, planarity in the π-conjugated backbone is a necessary for crystallization that involves $\pi-\pi$ stacking.[47,48] Neutral polyacetylene modeled in the gas phase is planar, and all dihedral angles along C−C bonds are either 0° or 180°. The dihedral angle deviation ($\Delta\theta$) from this reference point (Figure 3a) is therefore a quantitative measure of the effect of substitution on planarity, with a higher $\Delta\theta$ indicating poorer planarity.

Beginning our study of planarity, we examined the difference between polyacetylene mono- and di- substituted with CF_3 groups (Figure 3b). In both cases, the magnitude of $\Delta\theta$ oscillates as each successive bond is either primarily a single or double bond, with single bonds enabling greater rotational freedom (Figure 3c). Disubstituted polyacetylene exhibits significantly larger oscillations, however, and overall exhibits significantly higher $\Delta\theta$ values. Qualitatively, disubstituted polyacetylene appears significantly more twisted and less planar than its monosubstituted counterpart, consistent with our quantitative analysis. Furthermore, while the disubstituted derivative possesses the same π^* orbital energy (−5.3 eV) (Table 1, entries 5 and 6) as its monosubstituted counterpart, its $\Delta\pi-\pi^*$ is more than twice as wide as the monosubstituted derivative (3.2 vs 1.4 eV). This implies that disubstituted polyacetylene is less attractive as a synthetic candidate as a consequence of significant backbone distortion. Indeed, a similar trend is observed for −CN disubstituted polyacetylene derivatives (Table 1, entries 8 and 9; SI, Table S1, entries

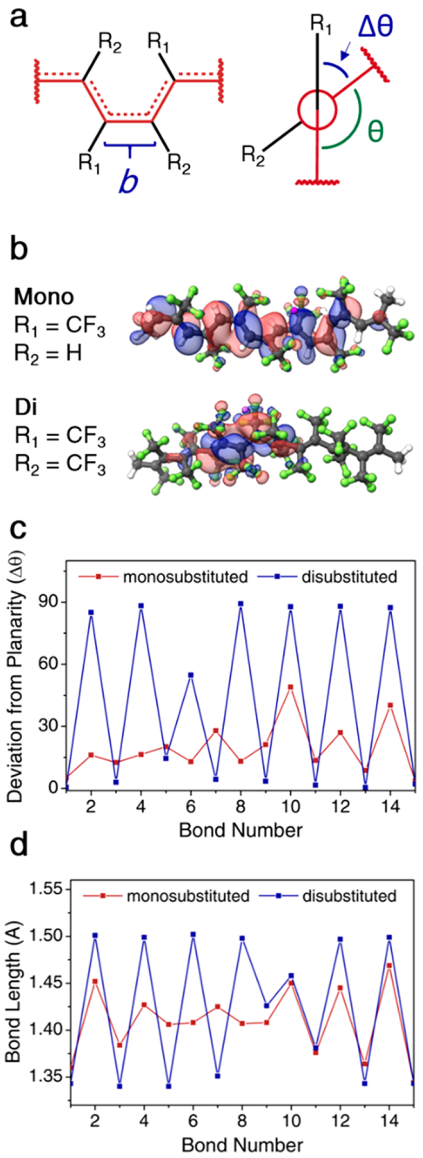

Figure 3. Measuring polymer geometry. (a) The model polymer, with the bond length (b) and dihedral angle deviation ($\Delta\theta$) highlighted for clarity. (b) Representation of the π^* molecular orbital of mono- and disubstituted polyacetylenes, functionalized with CF_3. Carbon atoms are shown in gray, hydrogen in white, and fluorine in green. (c) Dihedral angle deviation from planarity, comparing mono- (red) and disubstituted (blue), $-CF_3$ functionalized polyacetylene. (d) BLA pattern of mono- (red) and disubstituted (blue) polyacetylenes, functionalized with CF_3. Lines connecting dots included as a guide for the eye.

S15−18). However, it is important to also consider the nature of soliton formation prior to a decisive judgment.

Delocalized soliton formation is critical to achieving high conductivity in polyacetylene. We can use bond length alternation (BLA) patterns to quantify the formation of a soliton, examining the carbon−carbon bond lengths (b) along the polymer backbone.[49] Neutral polyacetylene has alternating single and double bonds in its backbone as a consequence of Peierls instability,.[50] When a soliton is formed, these bonds converge on a single value, indicating partial single/double bond character along the polymer backbone. Were the entire backbone to converge on the same bond length, the semiconducting nature of polyacetylene would break down

https://doi.org/10.1021/acs.jpclett.1c01925
J. Phys. Chem. Lett. 2021, 12, 7745−7751

Table 1. Summarized Quantitative Measures of the Properties of Polyacetylene Derivatives[a]

entry	R_1	R_2	π^* (eV)	$\Delta\pi-\pi^*$ (eV)	$\Delta\theta_{av}$ (deg)	b_{av} (Å)	$\sigma_b \times 10^{-2}$
1	−H	−H	−3.3	1.4	2.4	1.40	3.0
2	$-CO_2CH_3$	−H	−4.7	1.4	15.4	1.41	3.9
3	$-C_6F_5$	−H	−4.8	1.2	4.8	1.41	2.9
4	$-C_6H_4NO_2$	−H	−5.1	1.7	19.9	1.41	4.6
5	$-CF_3$	−H	−5.3	1.4	19.2	1.41	3.7
6	$-CF_3$	$-CF_3$	−5.3	3.2	40.7	1.42	7.4
7	$-CF_2CF_3$	−H	−5.3	1.9	21.9	1.41	4.8
8	−CN	−H	−5.5	1.0	5.3	1.41	2.6
8	−CN	−CN	−7.0	1.5	22.9	1.42	4.4

[a] π^* = the energy of the π^* MO. $\Delta\pi-\pi^*$ = the energy difference between the π and π^* orbitals. $\Delta\theta_{av}$ = average deviation in dihedral angle from planar structure. b_{av} = average carbon−carbon bond length. σ_b = standard deviation in carbon−carbon bond lengths.

as the π and π^* orbitals converge to form a metallic state.[15] BLA patterns (Figure 3d) indicate that disubstitution results in a less delocalized soliton extending over, at most, two bonds, while monosubstitution results in a larger soliton extending over at least six bonds. This may be attributed to the disubstituted oligomer's shielding effect on the counterion, destabilizing the formation of a soliton, or to a distortive steric effect caused by the density of substituents. Regardless, not only does disubstitution result in less planarity, it also appears to prevent delocalized soliton formation. These results strongly imply that substituent density should be low to maintain high polymer conductivity.

Focusing next on monosubstituted derivatives, we sought to understand substituent size. To this end, we directly compared the CF_3 and CF_2CF_3 substituents. Both substituents result in the same π^* orbital energy, but the CF_2CF_3 derivative exhibits a significantly wider $\Delta\pi-\pi^*$ than the CF_3 derivative (1.9 vs 1.4 eV) (Figure 2). We hypothesized that greater steric effects due to the larger substituent distort polymer backbone π-conjugation. However, we wanted to differentiate between steric and inductive effects. Energy calculations were thus performed, in which the CF_2CF_3 substituted polymer had its backbone fixed in the CF_3 optimized configuration (SI, Figures S14, S34). Under these fixed conditions, the π^* orbital remained unchanged while $\Delta\pi-\pi^*$ was decreased to 1.5 eV, which is attributed to more π-conjugation throughout the oligomer due to forced planarization. The additional electron-withdrawing fluorine atoms do not significantly contribute to π^* stabilization, and their main contribution is therefore steric, distorting the polyacetylene backbone and increasing $\Delta\pi-\pi^*$.

The extent to which each derivative meets criteria (i−iv) can be represented quantitatively (Table 1). The π^* molecular orbital energy (i) and $\Delta\pi-\pi^*$ (ii) are straightforward, with a low value for each being desirable, as described above. The average deviation from planarity ($\Delta\theta_{av}$) accounts for backbone distortion, with a higher number representing a more distorted backbone. Polymers with a low $\Delta\theta_{av}$ best satisfy the polymer planarity criterion (iii). Relatedly, the average carbon−carbon bond length (b_{av}) is included as a rough measurement of steric repulsion between substituents as carbon atoms are forced further apart to accommodate large substituents. Finally, the standard deviation in carbon−carbon bond lengths (σ_b) describes the degree to which a delocalized soliton is formed (iv). This is because in a perfectly delocalized soliton the bond lengths would converge on a single value, and σ_b would approach zero; as bond-lengths differentiate between single and double bonds, σ_b increases. Therefore, we predict that a decreasing value of σ_b would correlate with an increasingly delocalized soliton and increasing charge conductivity.

On the basis of this quantitative data, CN-substituted polyacetylene appears to be the most interesting synthetic candidate (Figure 4). A couple of trends are notable. First,

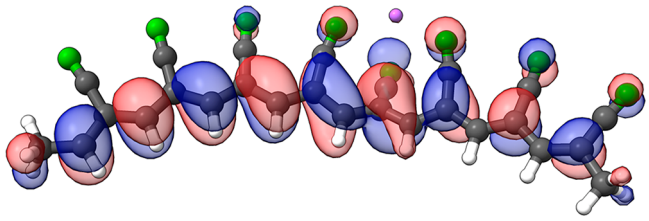

Figure 4. *n*-Doped polyacetylene monofunctionalized with cyano groups. Representation of the π^* molecular orbital of the polymer monofunctionalized with CN, which possesses a relatively planar backbone, a low π^* energy, a narrow $\Delta\pi-\pi^*$, and a delocalized soliton. Carbon atoms are shown in gray, hydrogen in white, nitrogen in green, and sodium in pink.

disubstituted polymers show consistently higher $\Delta\theta_{av}$ values. This increases $\Delta\pi-\pi^*$ for CN disubstituted polyacetylene, although it maintains a $\Delta\pi-\pi^*$ (1.5 eV) that is comparable to that of native polyacetylene (1.4 eV). Interestingly, CN has significantly lower $\Delta\theta_{av}$ and σ_b values than CF_3 (Table 1, entries 5 and 8), which is similarly small. We speculate that this is a consequence of hybridization; CN is *sp* hybridized and therefore less sterically bulky than sp^3-hybridized CF_3. Regardless, low $\Delta\theta_{av}$ and σ_b values suggest that the CN derivative possesses a high degree of planarity and soliton delocalization. In fact, solitons on polyacetylene that is monosubstituted with CN appear to be *more delocalized than native polyacetylene*, with a σ_b value of 2.6 compared to 3.0 for unsubstituted polyacetylene.

Another interesting substituent is PFP, which has an unusually planar structure despite the large substituent size (SI, Figure S5, entry S6). Although the π^* energy is above the reduction potential of O_2 in acidic conditions, the π^* is still below the O_2 reduction potential under neutral conditions. Moreover, the PFP derivative exhibits a narrow $\Delta\pi-\pi^*$ of 1.2 eV, the lowest $\Delta\theta_{av}$ of any derivative, and a low σ_b value that is comparable to native polyacetylene (Table 1, entry 2). This striking retention of planarity and soliton delocalization appears to be due to the planarity of PFP, which allows the phenyl rings to efficiently stack when the polymer is in its *trans* isomer. Indeed, the *p*NP derivative in its *trans* isomer has a significantly narrower $\Delta\pi-\pi^*$ (1.0 vs 1.7 eV in its *cis* isomer),

https://doi.org/10.1021/acs.jpclett.1c01925
J. Phys. Chem. Lett. 2021, 12, 7745−7751

has a lower π^* (−5.3 eV), is more planar, and exhibits a more delocalized soliton (SI, Table S1, entry S6). The *trans* isomer, however, is 76.3 kJ/mol less stable that its *cis* isomer and is not predicted to be the favored form. Furthermore, it should be noted that the bulkiness of the PFP substituent, as with other phenyl substituents, may prevent either isomer from effectively π-stacking, crystallizing, or forming meaningful intermolecular interactions regardless of planarity.

To conclude, we have developed a method for screening candidate polyacetylene derivatives for *n*-doped materials. Evaluating a range of mono- and disubstituted polymers, we have determined that polyacetylene monosubstituted with CN represents the most attractive synthetic candidate. However, on the basis of their predicted π^* orbital stabilization, $\Delta\pi-\pi^*$, planarity, or soliton delocalization, many other polyacetylene derivatives are also interesting candidates. Ultimately, it is important that more polyacetylene derivatives are synthesized overall so that this method can be further validated and improved by comparison to experimental data.

The clearest lesson of this study is the strong steric limitation on substituents. Other π-conjugated polymers, such as polythiophenes, polyfluorenes, and polyphenylenes can tolerate a wide range of substituents, often without significant backbone distortion.[51−53] Polyacetylene has both a smaller repeat unit and lacks planarizing aromaticity, and we predict that effective π-conjugation, delocalized charge carriers (solitons), and highly conductive materials will therefore require especially small substituents. The primary exception to this is planar, phenyl substituents, for which it is possible to access stable and planar *trans* polyacetylene derivatives. Indeed, *sp* and sp^2 hybridized substituents also enabled resonance with the backbone and extension of the π system; this decreases $\Delta\pi-\pi^*$ and the π^* orbital energy, further improving the stability of the derivative to oxidation. Overall, we believe that these insights will inform the synthesis and development of new polyacetylene derivatives and open the door to the rigorous study and application of *n*-doped polyacetylene.

METHODS

Oligomers were modeled with eight repeat units, following previous work showing that oligomeric structures of this length approach the saturation length of electronic properties for π-conjugated polymers.[54−56] Density functional theory (DFT) calculations were implemented in Gaussian 16, using the nonlocal hybrid Becke three parameter Lee−Yang−Parr (B3LYP) functional.[57−61] The split-valence double-ζ basis set 6-31(d,p) was used for geometric optimization. The π and π^* energy values were found using the larger split-valence triple-ζ basis set, 6-311+G(d,p), through a single-point energy calculation.[62,63] Charged species were modeled as a one-dimensional oligomer paired with a sodium atom and in a doublet spin state. Unsubstituted polyacetylene was modeled in the gas phase with and without implicit solvation by *n*-hexanes (ε = 1.8819), tetrahydrofuran (ε = 7.4257), dichloromethane (ε = 8.93), and acetonitrile (ε = 35.688).[64−66] Because of better agreement between the gas phase calculations and the experimental $\Delta\pi-\pi^*$ (SI, Table S2), the remaining charged species were modeled in the gas phase. We additionally chose this approximation for our calculations because polyacetylene acts as a one-dimensional topological insulator.[67,68]

ASSOCIATED CONTENT

Supporting Information

The Supporting Information is available free of charge at https://pubs.acs.org/doi/10.1021/acs.jpclett.1c01925.

Table of calculated properties, images, bond length alternation patterns, and dihedral angles for all polymers in this study and additional potential energy diagrams (PDF)

AUTHOR INFORMATION

Corresponding Author

Dwight S. Seferos − *Department of Chemistry, University of Toronto, Toronto, Ontario M5S 3H6, Canada; Department of Chemical Engineering and Applied Chemistry, University of Toronto, Toronto, Ontario M5S 3E5, Canada;* orcid.org/0000-0001-8742-8058; Email: dwight.seferos@utoronto.ca

Authors

Liam D. P. Foyle − *Department of Chemistry, University of Toronto, Toronto, Ontario M5S 3H6, Canada*

Garion E. J. Hicks − *Department of Chemistry, University of Toronto, Toronto, Ontario M5S 3H6, Canada*

Adam A. Pollit − *Department of Chemistry, University of Toronto, Toronto, Ontario M5S 3H6, Canada*

Complete contact information is available at: https://pubs.acs.org/10.1021/acs.jpclett.1c01925

Author Contributions

L.D.P.F. and G.E.J.H. contributed equally to this work. G.E.J.H. and D.S.S. designed the study. L.D.P.F. performed all calculations. All authors contributed to write the manuscript.

Notes

The authors declare no competing financial interest.

ACKNOWLEDGMENTS

This work was supported by the University of Toronto, NSERC, the CFI, and the Ontario Research Fund. D.S.S. is grateful to the Connaught Foundation for the McLean Award and NSERC for the E. W. R. Steacie Memorial Fellowship.

REFERENCES

(1) Bronstein, H.; Nielsen, C. B.; Schroeder, B. C.; McCulloch, I. The Role of Chemical Design in the Performance of Organic Semiconductors. *Nat. Rev. Chem.* **2020**, *4* (2), 66−77.

(2) Coates, G. W.; Getzler, Y. D. Y. L. Chemical Recycling to Monomer for an Ideal, Circular Polymer Economy. *Nat. Rev. Mater.* **2020**, *5* (7), 501−516.

(3) Feig, V. R.; Tran, H.; Bao, Z. Biodegradable Polymeric Materials in Degradable Electronic Devices. *ACS Cent. Sci.* **2018**, *4* (3), 337−348.

(4) Li, W.; Liu, Q.; Zhang, Y.; Li, C.; He, Z.; Choy, W. C. H.; Low, P. J.; Sonar, P.; Kyaw, A. K. K. Biodegradable Materials and Green Processing for Green Electronics. *Adv. Mater.* **2020**, *32*, 2001591.

(5) Rasmussen, S. C. Conjugated and Conducting Organic Polymers: The First 150 Years. *ChemPlusChem* **2020**, *85* (7), 1412−1429.

(6) Guo, X.; Facchetti, A. The Journey of Conducting Polymers from Discovery to Application. *Nat. Mater.* **2020**, *19* (9), 922−928.

(7) Nair, N. M.; Pakkathillam, J. K.; Kumar, K.; Arunachalam, K.; Ray, D.; Swaminathan, P. Printable Silver Nanowire and PEDOT:PSS

Nanocomposite Ink for Flexible Transparent Conducting Applications. *ACS Appl. Electron. Mater.* **2020**, *2* (4), 1000−1010.
(8) Dominguez-Alfaro, A.; Gabirondo, E.; Alegret, N.; De León-Almazán, C. M.; Hernandez, R.; Vallejo-Illarramendi, A.; Prato, M.; Mecerreyes, D. 3D Printable Conducting and Biocompatible PEDOT- Graft -PLA Copolymers by Direct Ink Writing. *Macromol. Rapid Commun.* **2021**, *42*, 2100100.
(9) Dauzon, E.; Lin, Y.; Faber, H.; Yengel, E.; Sallenave, X.; Plesse, C.; Goubard, F.; Amassian, A.; Anthopoulos, T. D. Stretchable and Transparent Conductive PEDOT:PSS-Based Electrodes for Organic Photovoltaics and Strain Sensors Applications. *Adv. Funct. Mater.* **2020**, *30* (28), 2001251.
(10) Lee, J. H.; Jeong, Y. R.; Lee, G.; Jin, S. W.; Lee, Y. H.; Hong, S. Y.; Park, H.; Kim, J. W.; Lee, S.-S.; Ha, J. S. Highly Conductive, Stretchable, and Transparent PEDOT:PSS Electrodes Fabricated with Triblock Copolymer Additives and Acid Treatment. *ACS Appl. Mater. Interfaces* **2018**, *10* (33), 28027−28035.
(11) Lindorf, M.; Mazzio, K. A.; Pflaum, J.; Nielsch, K.; Brütting, W.; Albrecht, M. Organic-Based Thermoelectrics. *J. Mater. Chem. A* **2020**, *8* (16), 7495−7507.
(12) Yang, J. C.; Mun, J.; Kwon, S. Y.; Park, S.; Bao, Z.; Park, S. Electronic Skin: Recent Progress and Future Prospects for Skin-Attachable Devices for Health Monitoring, Robotics, and Prosthetics. *Adv. Mater.* **2019**, *31*, 1904765.
(13) Heo, D. N.; Lee, S.-J.; Timsina, R.; Qiu, X.; Castro, N. J.; Zhang, L. G. Development of 3D Printable Conductive Hydrogel with Crystallized PEDOT:PSS for Neural Tissue Engineering. *Mater. Sci. Eng., C* **2019**, *99*, 582−590.
(14) Sultana, N.; Chang, H. C.; Jefferson, S.; Daniels, D. E. Application of Conductive Poly(3,4-Ethylenedioxythiophene):Poly-(Styrenesulfonate) (PEDOT:PSS) Polymers in Potential Biomedical Engineering. *J. Pharm. Invest.* **2020**, *50* (5), 437−444.
(15) Swager, T. M. 50th Anniversary Perspective : Conducting/Semiconducting Conjugated Polymers. A Personal Perspective on the Past and the Future. *Macromolecules* **2017**, *50* (13), 4867−4886.
(16) Ferguson, A. J.; Reid, O. G.; Nanayakkara, S. U.; Ihly, R.; Blackburn, J. L. Efficiency of Charge-Transfer Doping in Organic Semiconductors Probed with Quantitative Microwave and Direct-Current Conductance. *J. Phys. Chem. Lett.* **2018**, *9* (23), 6864−6870.
(17) Bubnova, O.; Crispin, X. Towards Polymer-Based Organic Thermoelectric Generators. *Energy Environ. Sci.* **2012**, *5* (11), 9345.
(18) MacDiarmid, A. G. Synthetic Metals": A Novel Role for Organic Polymers (Nobel Lecture). *Angew. Chem., Int. Ed.* **2001**, *40* (14), 2581−2590.
(19) Shirakawa, H.; Louis, E. J.; MacDiarmid, A. G.; Chiang, C. K.; Heeger, A. J. Synthesis of Electrically Conducting Organic Polymers: Halogen Derivatives of Polyacetylene, (CH)X. *J. Chem. Soc., Chem. Commun.* **1977**, 578−580.
(20) Shirakawa, H. The Discovery of Polyacetylene Film: The Dawning of an Era of Conducting Polymers (Nobel Lecture). *Angew. Chem., Int. Ed.* **2001**, *40* (14), 2574−2580.
(21) Chiang, C. K.; Fincher, C. R.; Park, Y. W.; Heeger, A. J.; Shirakawa, H.; Louis, E. J.; Gau, S. C.; MacDiarmid, A. G. Electrical Conductivity in Doped Polyacetylene. *Phys. Rev. Lett.* **1977**, *39* (17), 1098−1101.
(22) Boswell, B. R.; Mansson, C. M. F.; Cox, J. M.; Jin, Z.; Romaniuk, J. A. H.; Lindquist, K. P.; Cegelski, L.; Xia, Y.; Lopez, S. A.; Burns, N. Z. Mechanochemical Synthesis of an Elusive Fluorinated Polyacetylene. *Nat. Chem.* **2021**, *13* (1), 41−46.
(23) Peterson, G. I.; Yang, S.; Choi, T. L. Synthesis of Functional Polyacetylenes via Cyclopolymerization of Diyne Monomers with Grubbs-Type Catalysts. *Acc. Chem. Res.* **2019**, *52* (4), 994−1005.
(24) Lam, J. W. Y.; Tang, B. Z. Functional Polyacetylenes. *Acc. Chem. Res.* **2005**, *38* (9), 745−754.
(25) Kang, C.; Jung, K.; Ahn, S.; Choi, T.-L. Controlled Cyclopolymerization of 1,5-Hexadiynes to Give Narrow Band Gap Conjugated Polyacetylenes Containing Highly Strained Cyclobutenes. *J. Am. Chem. Soc.* **2020**, *142* (40), 17140−17146.
(26) Langsdorf, B. L.; Zhou, X.; Adler, D. H.; Lonergan, M. C. Synthesis and Characterization of Soluble, Ionically Functionalized Polyacetylenes. *Macromolecules* **1999**, *32* (8), 2796−2798.
(27) Robinson, S. G.; Lonergan, M. C. Polyacetylene p−n Junctions with Varying Dopant Density by Polyelectrolyte-Mediated Electrochemistry. *J. Phys. Chem. C* **2013**, *117* (4), 1600−1610.
(28) Cheng, C. H. W.; Boettcher, S. W.; Johnston, D. H.; Lonergan, M. C. Unidirectional Current in a Polyacetylene Hetero-Ionic Junction. *J. Am. Chem. Soc.* **2004**, *126* (28), 8666−8667.
(29) Wang, Y.; Hao, W.; Huang, W.; Zhao, H.; Zhu, J.; Fang, W. Tuning the Ambipolar Character of Copolymers with Substituents: A Density Functional Theory Study. *J. Phys. Chem. Lett.* **2020**, *11* (10), 3928−3933.
(30) Phan, H.; Kelly, T. J.; Zhugayevych, A.; Bazan, G. C.; Nguyen, T.-Q.; Jarvis, E. A.; Tretiak, S. Tuning Optical Properties of Conjugated Molecules by Lewis Acids: Insights from Electronic Structure Modeling. *J. Phys. Chem. Lett.* **2019**, *10* (16), 4632−4638.
(31) Osaka, I.; Zhang, R.; Liu, J.; Smilgies, D. M.; Kowalewski, T.; McCullough, R. D. Highly Stable Semiconducting Polymers Based on Thiazolothiazole. *Chem. Mater.* **2010**, *22* (14), 4191−4196.
(32) De Leeuw, D. M.; Simenon, M. M. J.; Brown, A. R.; Einerhand, R. E. F. Stability of N-Type Doped Conducting Polymers and Consequences for Polymeric Microelectronic Devices. *Synth. Met.* **1997**, *87* (1), 53−59.
(33) Wijsboom, Y. H.; Patra, A.; Zade, S. S.; Sheynin, Y.; Li, M.; Shimon, L. J. W.; Bendikov, M. Controlling Rigidity and Planarity in Conjugated Polymers: Poly(3,4-Ethylenedithioselenophene). *Angew. Chem.* **2009**, *121* (30), 5551−5555.
(34) Su, W. P.; Schrieffer, J. R.; Heeger, A. J. Solitons in Polyacetylene. *Phys. Rev. Lett.* **1979**, *42* (25), 1698−1701.
(35) Kaner, R. B.; Porter, S. J.; Nairns, D. P.; MacDiarmid, A. G. The Application of Electrochemistry to the Measurement of Selected Intrinsic Properties of Polyacetylene. *J. Chem. Phys.* **1989**, *90* (9), 5102−5107.
(36) Namazian, M.; Coote, M. L. Accurate Calculation of Absolute One-Electron Redox Potentials of Some Para-Quinone Derivatives in Acetonitrile. *J. Phys. Chem. A* **2007**, *111* (30), 7227−7232.
(37) Zhang, J. *PEM Fuel Cell Electrocatalysts and Catalyst Layers*; Zhang, J., Ed.; Springer London: London, 2008 .
(38) Vasudevan, D.; Wendt, H. Electroreduction of Oxygen in Aprotic Media. *J. Electroanal. Chem.* **1995**, *392* (1−2), 69−74.
(39) Alem, S.; Wakim, S.; Lu, J.; Robertson, G.; Ding, J.; Tao, Y. Degradation Mechanism of Benzodithiophene-Based Conjugated Polymers When Exposed to Light in Air. *ACS Appl. Mater. Interfaces* **2012**, *4* (6), 2993−2998.
(40) Louis, B.; Caubergh, S.; Larsson, P. O.; Tian, Y.; Scheblykin, I. G. Light and Oxygen Induce Chain Scission of Conjugated Polymers in Solution. *Phys. Chem. Chem. Phys.* **2018**, *20* (3), 1829−1837.
(41) Montilla, F.; Mallavia, R. On the Origin of Green Emission Bands in Fluorene-Based Conjugated Polymers. *Adv. Funct. Mater.* **2007**, *17* (1), 71−78.
(42) Roncali, J. Molecular Engineering of the Band Gap of π-Conjugated Systems: Facing Technological Applications. *Macromol. Rapid Commun.* **2007**, *28* (17), 1761−1775.
(43) Blanchard, P.; Brisset, H.; Illien, B.; Riou, A.; Roncali, J. Bridged Dithienylethylenes as Precursors of Small Bandgap Electrogenerated Conjugated Polymers. *J. Org. Chem.* **1997**, *62* (8), 2401−2408.
(44) Fratini, S.; Nikolka, M.; Salleo, A.; Schweicher, G.; Sirringhaus, H. Charge Transport in High-Mobility Conjugated Polymers and Molecular Semiconductors. *Nat. Mater.* **2020**, *19* (5), 491−502.
(45) Hynynen, J.; Kiefer, D.; Yu, L.; Kroon, R.; Munir, R.; Amassian, A.; Kemerink, M.; Müller, C. Enhanced Electrical Conductivity of Molecularly P-Doped Poly(3-Hexylthiophene) through Understanding the Correlation with Solid-State Order. *Macromolecules* **2017**, *50* (20), 8140−8148.
(46) Noriega, R.; Rivnay, J.; Vandewal, K.; Koch, F. P. V.; Stingelin, N.; Smith, P.; Toney, M. F.; Salleo, A. A General Relationship

https://doi.org/10.1021/acs.jpclett.1c01925
J. Phys. Chem. Lett. 2021, 12, 7745−7751

between Disorder, Aggregation and Charge Transport in Conjugated Polymers. *Nat. Mater.* **2013**, *12* (11), 1038−1044.
(47) Moser, M.; Hidalgo, T. C.; Surgailis, J.; Gladisch, J.; Ghosh, S.; Sheelamanthula, R.; Thiburce, Q.; Giovannitti, A.; Salleo, A.; Gasparini, N.; et al. Side Chain Redistribution as a Strategy to Boost Organic Electrochemical Transistor Performance and Stability. *Adv. Mater.* **2020**, *32*, 2002748.
(48) C. Faria, G.; Duong, D. T.; Da Cunha, G. P.; Selter, P.; Strassø, L. A.; Davidson, E. C.; Segalman, R. A.; Hansen, M. R.; Deazevedo, E. R.; Salleo, A. On the Growth, Structure and Dynamics of P3EHT Crystals. *J. Mater. Chem. C* **2020**, *8*, 8155−8170.
(49) Ramírez-Solís, A.; Zicovich-Wilson, C. M.; Kirtman, B. Periodic Hartree-Fock and Density Functional Theory Calculations for Li-Doped Polyacetylene Chains. *J. Chem. Phys.* **2006**, *124* (24), 244703.
(50) Heeger, A. J. Charge Storage in Conducting Polymers: Solitons, Polarons, and Bipolarons. *Polym. J.* **1985**, *17*, 201−208.
(51) Lutz, J. P.; Hannigan, M. D.; McNeil, A. J. Polymers Synthesized via Catalyst-Transfer Polymerization and Their Applications. *Coord. Chem. Rev.* **2018**, *376*, 225−247.
(52) Kynaston, E. L.; Fang, Y.; Manion, J. G.; Obhi, N. K.; Howe, J. Y.; Perepichka, D. F.; Seferos, D. S. Patchy Nanofibers from the Thin Film Self-Assembly of a Conjugated Diblock Copolymer. *Angew. Chem., Int. Ed.* **2017**, *56* (22), 6152−6156.
(53) Hollinger, J.; Jahnke, A. A.; Coombs, N.; Seferos, D. S. Controlling Phase Separation and Optical Properties in Conjugated Polymers through Selenophene−Thiophene Copolymerization. *J. Am. Chem. Soc.* **2010**, *132* (25), 8546−8547.
(54) McCormick, T. M.; Bridges, C. R.; Carrera, E. I.; Dicarmine, P. M.; Gibson, G. L.; Hollinger, J.; Kozycz, L. M.; Seferos, D. S. Conjugated Polymers: Evaluating DFT Methods for More Accurate Orbital Energy Modeling. *Macromolecules* **2013**, *46* (10), 3879−3886.
(55) Lawrence, J.; Goto, E.; Ren, J. M.; Mcdearmon, B.; Kim, D. S.; Ochiai, Y.; Clark, P. G.; Laitar, D.; Higashihara, T.; Hawker, C. J. A Versatile and Efficient Strategy to Discrete Conjugated Oligomers Scheme 1. Comparison of Traditional Iterative Coupling and Oligomer Separation Strategy. *J. Am. Chem. Soc.* **2017**, *139*, 13735−13739.
(56) Kim, Y.; Park, H.; Abdilla, A.; Yun, H.; Han, J.; Stein, G. E.; Hawker, C. J.; Kim, B. J. Chain-Length-Dependent Self-Assembly Behaviors of Discrete Conjugated Oligo(3-Hexylthiophene). *Chem. Mater.* **2020**, *32* (8), 3597−3607.
(57) Stephens, P. J.; Devlin, F. J.; Chabalowski, C. F.; Frisch, M. J. Ab Initio Calculation of Vibrational Absorption and Circular Dichroism Spectra Using Density Functional Force Fields. *J. Phys. Chem.* **1994**, *98* (45), 11623−11627.
(58) Becke, A. D. Density-functional Thermochemistry. III. The Role of Exact Exchange. *J. Chem. Phys.* **1993**, *98* (7), 5648−5652.
(59) Lee, C.; Yang, W.; Parr, R. G. Development of the Colle-Salvetti Correlation-Energy Formula into a Functional of the Electron Density. *Phys. Rev. B: Condens. Matter Mater. Phys.* **1988**, *37* (2), 785−789.
(60) Weigend, F.; Ahlrichs, R. Balanced Basis Sets of Split Valence, Triple Zeta Valence and Quadruple Zeta Valence Quality for H to Rn: Design and Assessment of Accuracy. *Phys. Chem. Chem. Phys.* **2005**, *7* (18), 3297.
(61) Vosko, S. H.; Wilk, L.; Nusair, M. Accurate Spin-Dependent Electron Liquid Correlation Energies for Local Spin Density Calculations: A Critical Analysis. *Can. J. Phys.* **1980**, *58* (8), 1200−1211.
(62) Petersson, G. A.; Bennett, A.; Tensfeldt, T. G.; Al-Laham, M. A.; Shirley, W. A.; Mantzaris, J. A Complete Basis Set Model Chemistry. I. The Total Energies of Closed-shell Atoms and Hydrides of the First-row Elements. *J. Chem. Phys.* **1988**, *89* (4), 2193−2218.
(63) Andersson, M. P.; Uvdal, P. New Scale Factors for Harmonic Vibrational Frequencies Using the B3LYP Density Functional Method with the Triple-ζ Basis Set 6-311+G(d,P). *J. Phys. Chem. A* **2005**, *109* (12), 2937−2941.
(64) Marenich, A. V.; Cramer, C. J.; Truhlar, D. G. Universal Solvation Model Based on Solute Electron Density and on a Continuum Model of the Solvent Defined by the Bulk Dielectric Constant and Atomic Surface Tensions. *J. Phys. Chem. B* **2009**, *113* (18), 6378−6396.
(65) Herbert, J. M. *Dielectric Continuum Methods for Quantum Chemistry*; Wiley Interdisciplinary Reviews: Computational Molecular Science; Blackwell Publishing Inc., 2021; p e1519 .
(66) Zhang, J.; Zhang, H.; Wu, T.; Wang, Q.; van der Spoel, D. Comparison of Implicit and Explicit Solvent Models for the Calculation of Solvation Free Energy in Organic Solvents. *J. Chem. Theory Comput.* **2017**, *13* (3), 1034−1043.
(67) Hernangómez-Pérez, D.; Gunasekaran, S.; Venkataraman, L.; Evers, F. Solitonics with Polyacetylenes. *Nano Lett.* **2020**, *20* (4), 2615−2619.
(68) Ramírez-Solís, A.; Kirtman, B.; Bernai-Jáquez, R.; Zicovich-Wilson, C. M. Periodic Density Functional Theory Calculations for Na-Doped Quasi-One-Dimensional Polyacetylene Chains. *J. Phys. Chem. C* **2008**, *112* (25), 9493−9500.

https://doi.org/10.1021/acs.jpclett.1c01925
J. Phys. Chem. Lett. 2021, 12, 7745−7751